Pyroelectronics: Novel device concepts based on nitride interfaces

G. Zandler, J. A. Majewski, and P. Vogl
Physik-Department and Walter Schottky Institut, Technische Universität München,
Am Coulombwall, D-85748 Garching, Germany
(Physics & Chemistry of Semiconductor Interfaces (PCIS-26), San Diego, Jan. 1999)

A key property of the nitrides is the fact that they possess large spontaneous and piezoelectric polarization fields that allow a significant tailoring of the carrier dynamics and optical properties of nitride devices. In this paper, based on first-principles calculations of structural and electronic properties of bulk nitrides and their heterostructure, we investigate the potential of this novel material class for modern device applications by performing self-consistent Monte-Carlo simulations. We demonstrate that the internal electric fields have a significant and favorable influence on the transistor characteristics.

I. INTRODUCTION

The strong internal electric fields in nitrides that result from their strong pyro- and piezoelectric constants[1] have a dramatic effect on the electronic and optical properties in these systems. So far, only few theoretical predictions on the carrier dynamics in nitride devices have been published.[2]

II. THEORY OF INTERNAL POLARIZATION FIELDS IN GAN AND ALN INTERFACES

The present systematic theoretical studies of structural and electronic properties of heteroepitaxial AlN/GaN interfaces and homoepitaxial stacking faults,[3] are based on a well-established first-principles total-energy pseudopotential method within the local-density-functional formalism.[4] The band offsets, the charge accumulation at the polar interfaces of the junctions, and the interface electronic states have been investigated, taking fully into account the effects of lattice relaxation and electric polarization.

A. Polarity of interfaces

In the following, we consider strained GaN layers that are grown pseudomorphically on cubic or wurtzite AlN substrate. For cubic heterostructures, we consider [001], [110], and [111], and for the wurtzite heterostructures [0001], [0$\overline{1}$10], and [$\overline{1}$2$\overline{1}$0] growth directions, respectively. In the case of stacking fault interfaces, we assume the growth axis to be the hexagonal c-axis ([0001] in wurtzite, [111] in zincblende).

The space group P6$_3$mc (C_{6v}^4) of wurtzite is compatible with a spontaneous polarization along the hexagonal c-axis. Therefore, the polarization can be of both pyroelectric and piezoelectric origin in wurtzite AlN and GaN, but only piezoelectric in the cubic phases. Whenever the polarization lies parallel to the growth direction, its change (divergence) across the interface is equivalent to an interface charge. Among the interfaces between GaN and AlN that we have studied, the [111] GaN/AlN, the [0001] GaN/AlN, and the stacking fault interface between the wurtzite and zincblende GaN interface are of this type that may be termed "polar". In cases such as [$\overline{1}$2$\overline{1}$0] GaN/AlN, [0$\overline{1}$10] GaN/AlN, or [110] GaN/AlN, on the other hand, the polarization lies parallel to the interface and therefore does not give rise to a charge accumulation. We term those interfaces "nonpolar". A limiting case of this type is the cubic [001] GaN/AlN interface.

Computationally, we have modeled all of these interfaces by supercells containing up to 40 atoms (for [0$\overline{1}$10] and [$\overline{1}$2$\overline{1}$0] wurtzite structures). All atomic positions in the unit cell have been optimized by minimizing the total energy via the Hellmann-Feynman forces. The length of the supercell was determined by minimizing the stress tensor component along the growth direction. Based on these first-principles calculations, we find that the charges induced at the interfaces and VBO's are insensitive to the lattice constant along the growth direction, but highly sensitive to the atomic relaxation at the interface (e.g. the VBO for the relaxed [0001] GaN/AlN interface is 0.4 eV smaller than for the unrelaxed one). The lattice relaxation near the interface reduces the interface charge approximately by a factor of two.

B. Valence band offsets and interface charges

The valence band offset ΔE_V at an interface between two semiconductors (or between two phases of one material) can be conveniently split up into two terms [5] $\Delta E_V = \Delta\overline{V} + \Delta E_{BS}$, where $\Delta\overline{V}$ is the asymptotic difference between the laterally and vertically averaged electrostatic potential $\overline{V}(z)$, and ΔE_{BS} is the bulk band structure contribution. For neutral interfaces, $\Delta\overline{V}$ equals the dipole moment of the electrostatic charge density $\overline{\rho}(z)$ across the interface. In the case of charged interfaces, the electrostatic charge density $\overline{\rho}(z)$ contains an additional monopole term that is proportional to the difference between the polarizations in the two adjacent materials. The monopole charge density causes the macroscopically

averaged electrostatic potential to change linearly with distance from the interface. This contribution can be filtered out[6] and the intrinsic $\Delta\overline{V}$ can be obtained, based on the remaining dipolar contribution to $\overline{\rho}(z)$. By integrating the monopole charge density across the interface, we have been able to calculate the charge induced at the interface σ. Finally, the conduction band offset ΔE_C is defined by $\Delta E_C = \Delta E_V + \Delta E_{gap}$, where ΔE_{gap} is the difference between the fundamental band gaps of two constituent bulk crystals.

The calculated band offsets and charges induced at polar interfaces are given in Table I, together with the individual contributions to the VBO's. The presently predicted VBO's agree very well with recent experimental data[7,8], but not with some core-level photoemission data that suggest an extremely high VBO of 1.36 eV.[9].

It is interesting to note that all calculated VBO's are of the order of 0.7 - 0.9 eV and are insensitive to the polar/nonpolar character of the interface. Thus, the macroscopic electric fields do not grossly alter or modify the intrinsic band offsets. The large difference between conduction band offsets in cubic and wurtzite GaN/AlN heterostructures is a consequence of the indirect energy gap ($\Gamma \to X$) in cubic AlN that is 1.4 eV smaller than the direct gap in wurtzite AlN.

All studied GaN/AlN interfaces and stacking faults are of type I, with the valence band lying higher and the conduction band being lower in GaN, and zincblende phase of the stacking fault, respectively. The large charges accumulated at the stacking fault interfaces result mainly from the spontaneous dielectric polarization of the hexagonal phase, whereas the strain-induced piezoelectric contribution is negligible. The induced charges are seen to be reduced by a factor of two by the relaxation of the atomic positions at the interface. The presently calculated charges compare well (the difference amounts to 15-20 %) with results estimated from bulk calculations previously.[1] The stacking faults can generate a persistent photoconductivity and they can be tuned to act either as excitonic traps or luminescence centers, depending on the width of the cubic layer.

TABLE I. Valence and conduction band offsets, ΔE_V [eV] and ΔE_C [eV], potential lineup's $\Delta\overline{V}$ [eV], and band structure contributions ΔE_{BS} [eV] for GaN/AlN heterostructures and stacking fault interfaces. For GaN/AlN heterostructures, all values are given relative to the band edges in AlN, whereas for stacking faults they are given relative to the band edges of the wurtzite phase. The conversion factor for σ [C/m^2] to cm^{-2} is 6.241×10^{14}.

	wurtzite GaN/AlN			zincblende GaN/AlN			stacking faults	
	[0001]	[01̄10]	[1̄21̄0]	[001]	[110]	[111]	AlN	GaN
ΔE_{BS}	-0.26	-0.15	-0.17	-0.15	-0.15	0.13	-0.25	-0.046
$\Delta\overline{V}$	0.93	0.88	0.97	0.89	1.07	0.77	0.27	0.081
ΔE_V	0.67	0.73	0.80	0.75	0.92	0.90	0.02	0.04
ΔE_C	-1.92	-1.72	-1.67	-0.62	-0.51	-0.53	-1.30	-0.17
σ	0.010	0	0	0	0	0.006	0.009	0.003

Our calculations reveal the existence of large internal electric fields. Their influence on the properties of the electronic devices will be presented in subsequent sections.

III. MONTE-CARLO CALCULATIONS

A. Bulk transport properties of AlGaN

In our Monte Carlo transport calculations, we have used band parameters[10] deduced from the electronic structure calculations described above and have taken into account scattering rates for ionized impurity, intra- and intervalley phonon scattering, acoustic, piezoelectric, polar optical phonon and alloy scattering.

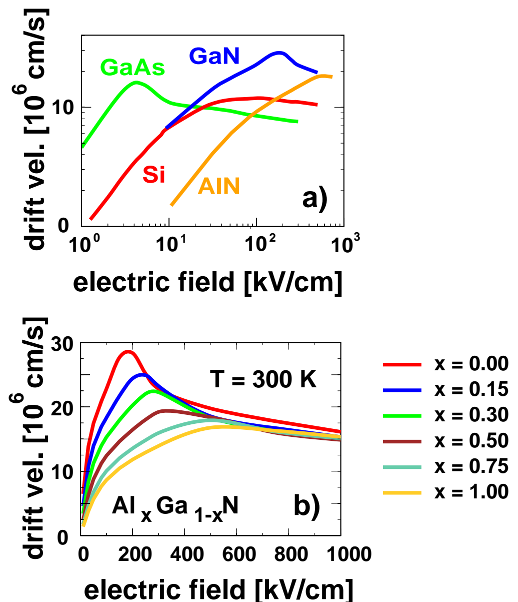

FIG. 1. (a) Calculated electron drift velocities of GaN and AlN in comparison with GaAs and Si. (b) Electron drift velocities in $Al_xGa_{1-x}N$ for various Al contents.

The resulting electron drift velocities (Fig. 1) at room temperature in bulk GaN both at low and high fields are in good agreement with other published theoretical results[11,12]. At high fields, GaN as well as AlN show a saturation velocity that is twice as high as in GaAs. For the $Al_xGa_{1-x}N$ material system, the heavier effective mass leads to considerably lower drift velocities at low fields, and to lower peak velocities with increasing Al content. As a consequence of the high phonon frequencies in both GaN and AlN on the other hand, the saturation velocities are predicted to be practically independent of the Al content, $\sim 1.5\times10^7$ cm/sec at 1 MV/cm namely. These results indicate that one can achieve much higher transit time frequencies in sub-micron nitride devices than in GaAs devices.

B. Pyroelectric and piezoelectric fields in wurtzite AlGaN/GaN single heterostructures

As discussed in section II, wurtzite structure III-Nitrides possess a pyroelectric polarization along the [0001] direction. Although the corresponding electric fields are of the order of some MV/cm[13], such fields are normally neutralized by unavoidable charged states at the surface of bulk samples. In heterostructures, however, each interface between different materials carries a charge that equals the divergence in the spontaneous and/or strain-induced piezoelectric polarization[14] across this interface. This charge cannot be compensated by charged states or free carriers.

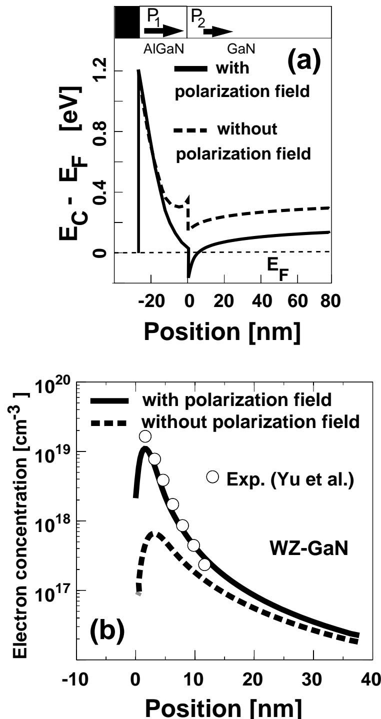

FIG. 2. Calculated results for a $Al_{.15}Ga_{.85}N$/GaN HFET with (full lines) and without (dashed lines) spontaneous and piezoelectric fields. A homogeneous n-doping background of 10^{16} cm^{-3} throughout the structure has been assumed. (a) Selfconsistently computed conduction band edge profile along the growth direction. (b) Calculated electron density profile in comparison with published experimental values.

To study the effect of this polarization induced interface charge on carrier transport and heterostructure device characteristics, we focus on a single $Al_{15}Ga_{85}N/GaN$ heterostructure (see Fig.2) first. In a tensile strained 30 nm thick $Al_{15}Ga_{85}N$ layer on GaN substrate, there is both a pyro- and a piezoelectrical polarization, while the relaxed 300 nm thick GaN layer only contains a pyroelectric moment. Assuming charge neutrality for the whole structure, there is a polarization induced charge density σ at the $Al_{15}Ga_{85}N/GaN$ interface and a compensating charge of $-\sigma/2$ at the surface and at the nucleation layer. We take σ to be $6{\cdot}10^{12}$ cm^{-2} which interpolates between a recent experimental value[14] $4{\cdot}10^{12}$ cm^{-2} and the theoretical value[13]) $8{\cdot}10^{12}$ cm^{-2}.

In Fig.2, we depict the selfconsistent band edge and density profiles along the growth direction, as obtained from a coupled 1-dimensional Schrödinger and Poisson equation. The Poisson equation includes all interface charges that result from the polarization fields. The bulk conduction band is modeled by a nonparabolic isotropic band centered at wave vector $\mathbf{k}$=0 in the wurtzite structure of GaN.[15,16,10] We have included up to 40 electronic subband energies and wave functions. As shown in Fig.2, the polarization induced positive interface charge causes a stronger confinement of two dimensional (2D) channel electron and an increase in the channel density by more than an order of magnitude. This is consistent with the experimental values for this layer structure shown in the figure. Furthermore, we have performed ensemble Monte Carlo calculations for drift mobilities along the channel that forms parallel to the interface. The inter- and intra-subband-scattering rates[17] have been determined consistently with the confined electronic channel states. We find excellent agreement between experimental and calculated temperature dependent mobilities[17], consistent with the high channel densities reported for these devices.[14,18] We would like to stress that such type of agreement strongly supports the existence of the strong pyroelectric polarization fields. For channel densities exceeding 10^{13} cm^{-2}, we predict a phonon limited drift mobility for 2D electrons close to 2000 cm^2/Vs for high quality interfaces, in good agreement with recent data on such structures.[19]

C. Influence of polarization fields on device performance

To study the influence of polarization fields on device characteristics, we have performed selfconsistent two-dimensional Monte Carlo simulations of various nitride based heterostructure devices.[10] At high bias voltages, it suffices to use a bulk description for the hot carrier transport in the channel layers.

In accordance with the high channel densities, the drain currents in such devices can become extraordinarily high. We have studied a 300nm gate length single heterostructure device with the same layer sequence as described above, but with additional doping densities of 10^{18} cm^{-3} in the supply layer. This results in channel densities of $8{\cdot}10^{12}$ cm^{-2} in the ungated structure. For this device, we find drains currents at open channel conditions up to 2000 A/m and predict a maximum transconductance of 430 S/m. Although the polarization induced interface charge in these devices suppresses parasitic substrate currents very efficiently, the magnitude of the threshold voltage is still fairly high (-6 V), mainly as a consequence of the high gate to channel separation of 30 nm.

Based on these bulk results, we have carried out self-consistent Monte Carlo simulations for planar short channel HFET's (heterostructure field effect transistors)[20]. We predict the following layer sequence to be well suited for high speed power applications. Beneath the contacts, we assume a highly doped $Al_{0.16}Ga_{0.84}N$ supply layer of 10 nm (4 nm with n= 1×10^{18} cm^{-3} and 6 nm with n = 1 $\times 10^{19}$ cm^{-3}). This is followed by an 8 nm $In_{0.05}Ga_{0.95}N$ channel with $n = 3 \times 10^{18}$ cm^{-3} and a subsequent 400 nm buffer layer that consists of $Al_{0.16}Ga_{0.84}N$. We assume this buffer layer to be fully compensated/nearly intrinsic, except for the first 6 nm that we take to be n-type with n = 2×10^{18} cm^{-3}. The intrinsic buffer is a prerequisite for obtaining an acceptable off-characteristics.

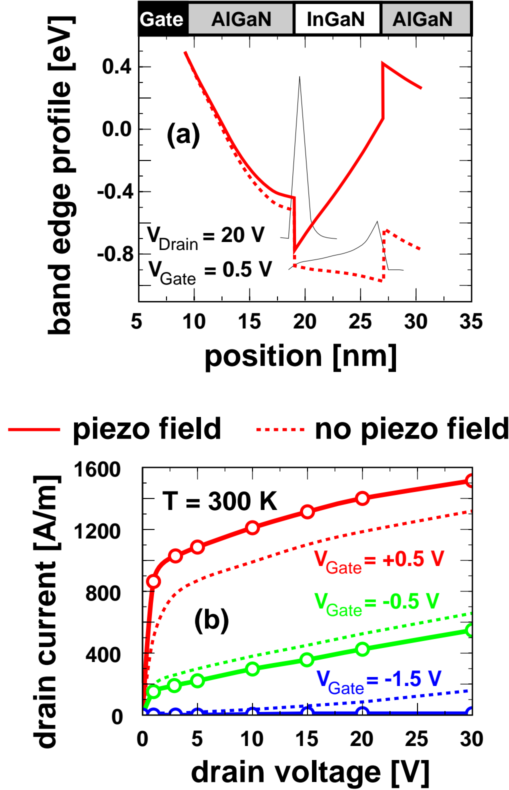

FIG. 3. Simulation results for a 300 nm gate length $In_{.05}Ga_{.95}N/Al_{.16}Ga_{.84}N$ HFET with (full lines and without (dashed lines) spontaneous and piezoelectric fields. (a) Selfconsistent conduction band edge profile and electron density. (b) Calculated drain current versus drain voltage for different gate voltages.

The lattice mismatch between the channel and the barrier material amounts to approximately 1%. This strain causes a macroscopic polarization of the channel in growth direction. The resulting electric field can be calculated from the piezoelectric tensor and the elastic constants. It amounts to 1.7×10^{8} V/m for the HFET layer sequence given above and is predicted to points towards the substrate. There is some experimental evidence for such polarization effects[21].

The influence of this huge polarization field on the drain current characteristics of a 300 nm gate HFET is shown in Fig. 3. The piezoelectric field pushes the electrons closer to the gate contact and therefore increases the transconductance from 650 S/m to 980 S/m (see Fig. 4. Furthermore, this confining effect improves the turn off behavior of the device considerably.

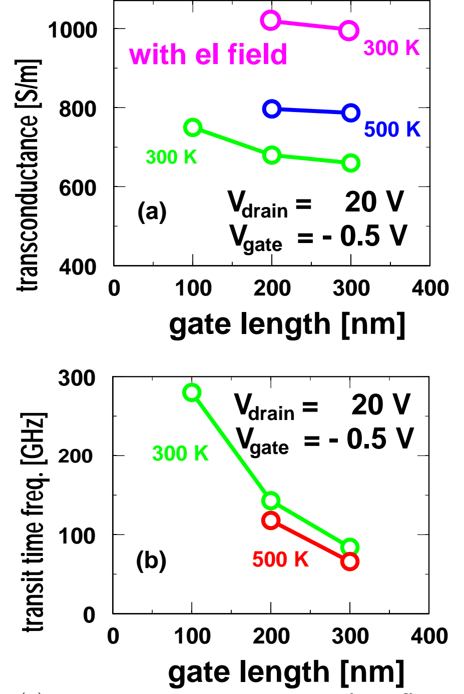

FIG. 4. (a) Calculated transconductance for different temperatures versus gate length of a $In_{.05}Ga_{.95}N/Al_{.16}Ga_{.84}N$ HFET with and without interface strain induced piezoelectric fields. (b) Predicted transit time frequency as a function of gate length and temperature at a drain voltage of 20 V and open channel conditions.

Our calculations predict average channel velocities exceeding 2×10^{5} m/s for gate lengths below 200 nm. The resulting transit time frequencies are depicted in Fig. 4(b) as a function of the gate length. The Monte Carlo calculations yield transit time frequencies of 120 GHz for gate lengths between 200 and 300 nm and up to 300 GHz for 100 nm gate length. Velocity overshoot is found to remain small in all of these cases but the turn-off behavior is poor for very short gate lengths. These short channel effects become even more pronounced at elevated temperatures. In conlusion, we predict excellent high frequency and power performance for wide-gap nitride based HFET's with gate lengths larger than 200 nm.

Polarization induced internal fields can be effectively utilized to tailor devices with optimal potential barriers towards the substrate. Indeed, we have theoretically designed the following inverted HEMT structure that should yield high channel densities and an excellent turn-off behavior. On top of a relaxed GaN buffer, there is a 12 nm thick strained $Al_{40}Ga_{80}N$ layer. The inner part (8 nm) of this layer is highly n-doped with $1.9 \cdot 10^{19}$ cm^{-3}. The remaining part of the barrier is lowly doped with $10^{17} cm^{-3}$ carriers. On top of this layer, there is a 30 nm

GaN (n-doped with $4 \cdot 10^{16} cm^{-3}$). The gate is assumed to be recessed in order to achieve a small gate to channel separation of 14 nm. In this HFET, we assume the opposite polarity of the structure as in the previous example. The GaN is assumed to be field free, whereas the 2 GaN/AlGaN interfaces have opposite interface charges. We have estimated them from bulk calculations[13] and set them to $\pm 2 \cdot 10^{13}$ cm^{-2}. The calculated band edge profile, together with the confined electron density is shown in fig. 5(a) at midgate position.

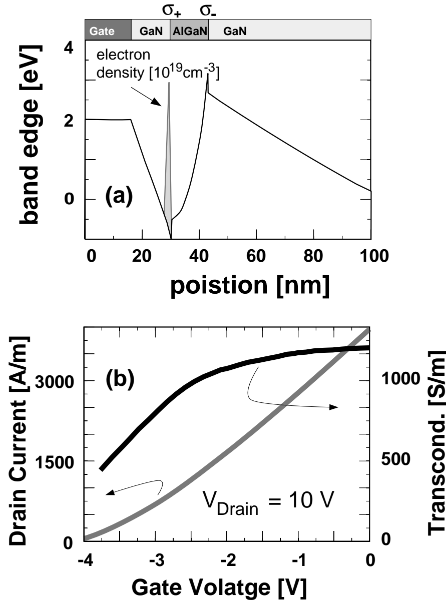

FIG. 5. Monte Carlo results for a 300 nm gate length inverted GaN/$Al_{40}Ga_{60}N$ HFET. (a) Selfconsistent band edge profile for -1V gate voltage and 10 V drain voltage. The channel electron density is indicated schematically. (b) Drain current and transconductance versus gate voltage at 10 V drain voltage.

As can be seen from fig.5, the polarization induced field produces a high potential barrier of approximately 3 eV towards the substrate. This has two major consequences. First, the highly doped AlGaN barrier gets completely depleted and all electrons are strongly confined in the channel that forms at the interface with the top GaN layer. Secondly, the high barrier completely suppresses the leakage current across the AlGaN barriers up to high voltages. We predict excellent electrical characteristics for such types of devices. In the present example, we find drain currents exceeding 3000 A/m and a transconductance that lies well above 1000 S/m. We note that the thickness of the AlGaN barrier layer and its doping level must be chosen carefully in order to avoid the formation of parasitic hole channels.

In conclusion, pyro- and piezoelectrical polarizations must be taken into account in order to explain experimentally observed mobilities and densities in nitride heterostructures. They are crucial for device performances and offer a unique possibility to design novel high power high frequency heterostructure transistors.

ACKNOWLEDGMENTS

This work has been supported by the Deutsche Forschungsgemeinschaft and the Bayerischer Forschungsverbund (FOROPTO).

---

[1] F. Bernardini, V. Fiorentini, and D. Vanderbilt, Phys. Rev. B **56**, R10024 (1997).
[2] J. A. Majewski, G. Zandler, and P. Vogl, Semiconductor Science and Technology **13**, 90 (1998).
[3] X. H. Wu, L. M. Brown, D. Kapolnek, S. Keller, B. Keller, S. P. DenBaars, and J. S. Speck, J. Appl. Phys. **80**, 3228 (1996); Z. Liliental-Weber, C. Kisielowski, S. Ruvimov, Y. Chen, J. Washburn, I. Grzegory, M. Bockowski, J. Jun, and S. Porowski, J. Electron. Mater. **25**, 1545 (1996).
[4] M. Städele, J. A. Majewski, and P. Vogl, Phys. Rev. B **56**, 6911 (1997); J. A. Majewski, M. Städele, and P. Vogl, MRS Internet J. Nitride Semicond. Res. **1**, 30 (1996).
[5] A. Baldereschi, S. Baroni, and R. Resta, Phys. Rev. Lett. **61**, 734 (1988).
[6] F. Bernardini and V. Fiorentini, Phys. Rev. B **57**, R9427 (1998).
[7] G. Martin, A. Botchkarev, A. Rockett, and H. Morkoç, Appl. Phys. Lett. **68**, 2541 (1996).
[8] G. Martin, S. Strite, A. Botchkarev, A. Agarwal, A. Rockett, H. Morkoç, W. R. L. Lambrecht, and B. Segall, Appl. Phys. Lett. **65**, 610 (1994).
[9] J. R. Waldrop and R. W. Grant, Appl. Phys. Lett. **68**, 2879 (1996).
[10] G. Zandler, J. A. Majewski, M. Stdele, P. Vogl, and F. Compagnone, Phys. Stat. Sol. (b) **204**, 133 (1997).
[11] U. V. Bhapkar, M. S. Shur, J. Appl. Phys. **82**, 1649 (1997).
[12] S. K. O'Leary, B. E. Foutz, M. S. Shur, U. V. Bhapkar, and L. F. Eastman, Solid State Commun. **105**, 621 (1988).
[13] F. Bernardini, V. Fiorentini, and D. Vanderbilt, Phys. Rev. B **56**, 10024 (1997).
[14] E. T. Yu, G. J. Sullivan, P. M. Asbeck, C. D. Wang, D. Qiao, and S. S. Lau, Appl. Phys. Lett. **71**, 2794 (1997).
[15] N. E. Christenson and I. Gorczyca, Phys. Rev. B **50**, 4397 (1994).
[16] K. Kim, W. R. L. Lambrecht, and B. Segall, Phys. Rev. B **53**, 16310 (1996).
[17] R. Oberhuber, G. Zandler, and P. Vogl, Appl. Phys. Lett. **73**(6), 818 (1998).
[18] Y. F. Wu, B. P. Keller, D. Kapolnek, P. Kozodoy, S. P. Denbaars and U. K. Mishra, Appl. Phys. Lett. **69**, 1438 (1996).
[19] R. Gaska, J. W. Yang, A. Osinsky, Q. Chen, M. A. Khan, A. O. Orlov, G. L. Snider, and M. S. Shur, Appl. Phys. Lett. **72**, 707 (1998).
[20] M. S. Shur and M. Asif Khan, MRS Bulletin **22**, 44 (1997).
[21] G. Martin, A. Botchkarev, A. Rockett, and H. Morkoç, Appl. Phys. Lett. **68**, 2541 (1996).